# Bandgap Engineering of Strained Monolayer and Bilayer MoS$_2$

Hiram J. Conley,[†] Bin Wang,[†] Jed I. Ziegler,[†] Richard F. Haglund, Jr.,[†] Sokrates T. Pantelides,[†,‡] and Kirill I. Bolotin*,[†]

[†]Department of Physics and Astronomy, Vanderbilt University, Nashville, Tennessee 37235, United States
[‡]Materials Science and Technology Division, Oak Ridge National Laboratory, Oak Ridge, Tennessee 37831, United States

Ⓢ Supporting Information

ABSTRACT: We report the influence of uniaxial tensile mechanical strain in the range 0−2.2% on the phonon spectra and bandstructures of monolayer and bilayer molybdenum disulfide (MoS$_2$) two-dimensional crystals. First, we employ Raman spectroscopy to observe phonon softening with increased strain, breaking the degeneracy in the E' Raman mode of MoS$_2$, and extract a Grüneisen parameter of ~1.06. Second, using photoluminescence spectroscopy we measure a decrease in the optical band gap of MoS$_2$ that is approximately linear with strain, ~45 meV/% strain for monolayer MoS$_2$ and ~120 meV/% strain for bilayer MoS$_2$. Third, we observe a pronounced strain-induced decrease in the photoluminescence intensity of monolayer MoS$_2$ that is indicative of the direct-to-indirect transition of the character of the optical band gap of this material at applied strain of ~1%. These observations constitute a demonstration of strain engineering the band structure in the emergent class of two-dimensional crystals, transition-metal dichalcogenides.

KEYWORDS: MoS$_2$, strain, bandgap engineering, photoluminescence, Grüneisen parameter
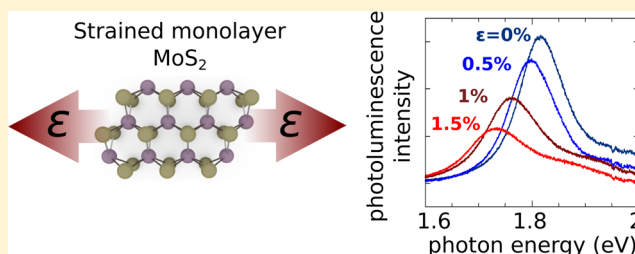
M onolayer (monolayer in this letter refers to one *molecular* molybdenum disulfide (MoS$_2$) layer or one layer of molybdenum atoms sandwiched between two layers of sulfur atoms; it is also sometimes referred to as trilayer MoS$_2$) molybdenum disulfide (MoS$_2$), along with other monolayer transition metal dichalcogenides (MoSe$_2$, WS$_2$, and WSe$_2$) have recently been the focus of extensive research activity that follows the footsteps of graphene, a celebrated all-carbon cousin of MoS$_2$.[1] Unlike semimetallic graphene, monolayer MoS$_2$ is a semiconductor with a large direct band gap.[2,3] The presence of a band gap opens a realm of electronic and photonic possibilities that have not been previously exploited in two-dimensional crystals and allows fabrication of MoS$_2$ transistors with an on/off ratio exceeding 10^8,[4,5] photodetectors with high responsivity,[6] and even LEDs.[7] Moreover, the direct nature of the band gap causes MoS$_2$ to exhibit photoluminescence at optical wavelengths[2,3] with intensity that is tunable via electrical gating.[8−10] Finally, strong Coulomb interactions between electrons and holes excited across the band gap of MoS$_2$ lead to the formation of tightly bound excitons that strongly affect the optical properties of this material.[9,10]

It has been well established that straining a two-dimensional material shifts its phonon modes, allowing a simple method to detect strain in these materials. These shifts, that are due to the anharmonicity of molecular potentials, can be probed with micro-Raman spectroscopy.[11,12] Very recently, it has been proposed that mechanical strain can strongly perturb the band structure of MoS$_2$. It has been predicted that straining MoS$_2$ modifies the band gap energy and the carrier effective masses.

Moreover, at strains larger than 1%, the lowest lying band gap changes from direct to indirect.[13−18] It has been suggested that strain engineering of the band structure of MoS$_2$ could be used to increase carrier mobility of MoS$_2$, to create tunable photonic devices and solar cells,[19] and even to control the magnetic properties of MoS$_2$.[13,14] While strain perturbs the band structure of all materials, two-dimensional materials such as MoS$_2$ can sustain strains greater than 11%,[20] allowing exceptional control of material properties by strain engineering.

Here, we investigate the influence of uniaxial tensile strain from 0% to 2.2% on the phonon spectra and band gaps of both monolayer and bilayer MoS$_2$, by employing a four point bending apparatus (Figure 1). First, with increasing strain, for both mono- and bilayer MoS$_2$, we observe splitting of the Raman peak due to the E' phonon mode into two distinct peaks that shift by 4.5 and 1 cm^{-1}/% strain. Second, a linear redshift of 45 meV/% strain of the position of the A peak in photoluminescence for monolayer MoS$_2$ (53 meV/% strain for bilayer MoS$_2$) indicates a corresponding reduction in band gap energy of these materials. Finally, we observe a pronounced strain-induced decrease in intensity of the photoluminescence of monolayer MoS$_2$. Our modeling and first-principles calculations indicate that this decrease is consistent with a transition of an optical band gap of MoS$_2$ from direct to
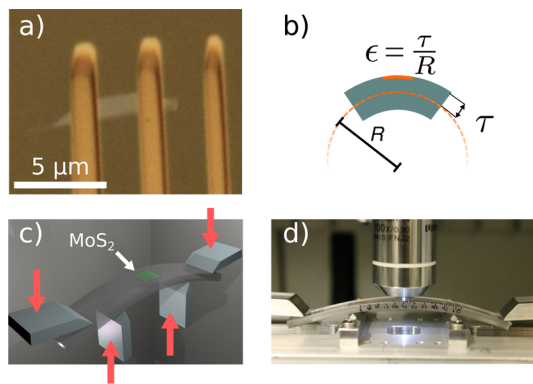
Figure 1. Straining MoS$_2$ devices. (a) Optical image of a bilayer MoS$_2$ flake with titanium clamps attaching it to SU8/polycarbonate substrate. (b,c) Schematic of the beam bending apparatus used to strain MoS$_2$. (d) Photograph of bending apparatus with MoS$_2$ under strain.

indirect at ∼1% strain, while the fundamental (or transport) band gap remains direct in the investigated regime of strain.

Fabrication of controllably strained devices starts by mechanically exfoliating[21] MoS$_2$ onto a layer of cross-linked SU8 photoresist deposited onto a polycarbonate beam. The number of layers of MoS$_2$ is verified using Raman microscopy.[22] Titanium clamps are then evaporated through a shadow mask to prevent MoS$_2$ from slipping against the substrate (Figure 1a). Uniaxial strain is applied to MoS$_2$ by controllably bending the polycarbonate beam in a four-point bending apparatus (Figure 1c,d). Assuming that as-fabricated exfoliated devices before bending are virtually strain-free,[23] we can calculate that upon bending the substrate with radius of curvature R, the induced strain in these devices is $\varepsilon = \tau/R$, where $2\tau = 2-3$ mm is the thickness of the substrate (Figure 1b).[12] Overall, we fabricated four monolayer and three bilayer MoS$_2$ devices. The strained devices are probed with a confocal microscope (Thermo Scientific DXR) that is used to collect both Raman and photoluminescence spectra. We employ a 532 nm laser excitation source with average power ∼100 μW, which does not damage our samples.

We first investigate the evolution of the Raman spectra of MoS$_2$ with strain (Figure 2). In unstrained monolayer MoS$_2$ devices, consistent with previous reports,[22,24] we observe the A' mode due to out-of-plane vibrations at 403 cm^{-1} and the
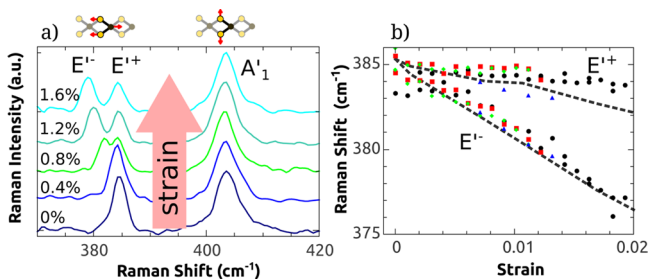
Figure 2. Phonon softening of single layer MoS$_2$. (a) Evolution of the Raman spectrum as a device is strained from 0 to 1.6%. (b) The peak location of the E'^+ and E'^- Raman modes, extracted by fitting the peaks to a Lorentzian, as their degeneracy is broken by straining MoS$_2$. Different colors represent individual devices. Dashed lines are the results of our first-principles calculations after subtraction of 9 cm^{-1} to account for underestimating phonon energies.

doubly degenerate E' mode due to in-plane vibrations of the crystal at 384 cm^{-1}.

With increased strain, the A' peak shows no measurable shift in position while the degenerate E' peak splits into two subpeaks (in contrast to a previous report[25]) that we label as E'^+ and E'^- (Figure 2), as strain breaks the symmetry of the crystal. The A' mode maintains its intensity as strain increases, while the total integrated intensity of the E' peaks now splits between the E'^+ and E'^- peaks. The E'^- peak shifts by 4.5 ± 0.3 cm^{-1}/% strain for monolayer devices and 4.6 ± 0.4 cm^{-1}/% strain for bilayer devices, while the E'^+ peak shifts by 1.0 ± 1 cm^{-1}/% strain for monolayer devices and 1.0 ± 0.9 cm^{-1}/% strain for bilayer devices, consistent with our first-principles calculations (dashed lines in Figure 2; details of the calculations can be found in the Supporting Information). For applied strain in the range 0−2%, the peak positions shift at nearly identical rates for all measured devices and do not exhibit hysteresis in multiple loading/unloading cycles, indicating that MoS$_2$ does not slip against the substrate and that the strain does not generate a significant number of defects. Bilayer devices behave in a similar manner but fail, either due to breaking or slipping of the MoS$_2$, at strains larger than 1%.

The strain dependence of the Raman E' mode enables us to calculate parameters characterizing anharmonicity of molecular potentials: the Grüneisen parameter, γ, and the shear deformation potential, β

$$\gamma_{E'} = -\frac{\Delta\omega_{E'^+} + \Delta\omega_{E'^-}}{2\omega_{E'}(1-\nu)\varepsilon} \tag{1}$$

$$\beta_{E'} = \frac{\Delta\omega_{E'^+} - \Delta\omega_{E'^-}}{\omega_{E'}(1+\nu)\varepsilon} \tag{2}$$

Here, ω is the frequency of the Raman mode, $\Delta\omega$ is the change of frequency per unit strain, and ν is Poisson's ratio, which for a material adhering to a substrate is the Poisson ratio of the substrate, 0.33.[12] This yields a Grüneisen parameter of 1.1 ± 0.2, half that of graphene (1.99)[12] and comparable to that of hexagonal boron nitride (0.95−1.2).[26,27] The shear deformation potential is 0.78 ± 0.1 for both monolayer and bilayer MoS$_2$.

Next, we investigate the evolution of the band structure of MoS$_2$ with strain through photoluminescence (PL) spectroscopy. The principal PL peak (A peak) in unstrained direct-gap monolayer MoS$_2$ at 1.82 ± 0.02 eV (Figure 3a) is due to a direct transition at the K point (Figure 3a, inset).[2,3] The B peak, due to a direct transition between the conduction band and a lower lying valence band, is obscured in our devices by background PL of polycarbonate/SU8. The PL spectra of unstrained indirect-band gap bilayer MoS$_2$ devices are characterized by a similar A peak at 1.81 ± 0.02 eV that originates from the same direct transition, but that is now less intense as it originates from hot luminescence. In addition, we observe an I peak at 1.53 ± 0.03 eV (Figure 3c), which originates from the transition across the indirect band gap of bilayer MoS$_2$ between the Γ and K points, (Figure 3c, inset).

Applied strain significantly changes the PL spectra (Figure 3a,c). For all measured monolayer devices, the A peak redshifts approximately linearly with strain, at a rate of 45 ± 7 meV/% strain (Figure 3b). For bilayer devices, the A and I peaks are red-shifted by 53 ± 10 and 129 ± 20 meV/% strain, respectively (Figure 3d). While the intensity of the A peak in monolayer devices decreases to a third of its original size with
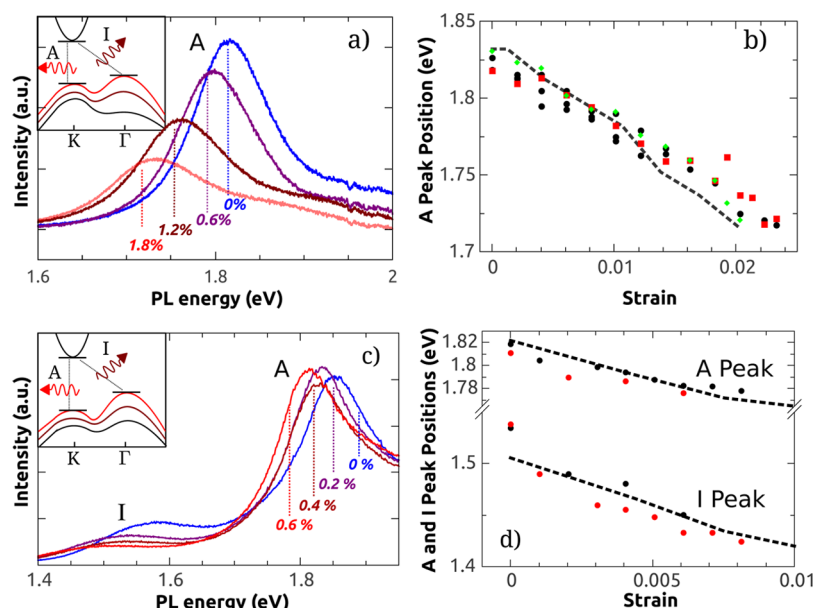
Figure 3. Photoluminescence spectra of strained MoS_2. (a) PL spectra of a representative monolayer device as it is strained from 0 to 1.8%. Strain independent PL background was subtracted. (b) Evolution of the position of the A peak of the PL spectrum (Lorentzian fits) with strain for several monolayer devices (colors represent different devices) with GW_0-BSE calculations (dashed line) of expected peak position after 25 meV offset. (c) PL spectra of a representative bilayer device as strain is increased from 0 to 0.6%. (d) PL peak position versus strain for the A and I peaks of bilayer devices (colors represent different devices) with good agreement to our GW_0-BSE calculations (dashed lines). Insets in panels a and b contain schematic representations of the band structure for both monolayer and bilayer MoS_2 devices that are progressively strained from 0% (black) to $\sim$5% (maroon) and $\sim$8% (red).

an applied strain of 2%, in bilayer devices the intensity of this peak is virtually strain-independent (Figure 4a).
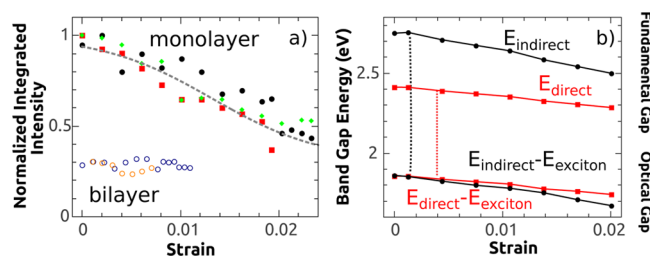
Figure 4. Direct to indirect band gap transition in MoS_2. (a) Evolution of intensity of the A peak of strained monolayer MoS_2 (solid shapes) with a fit (dashed curve) to the rate equations consistent with a degenerate direct and indirect optical band gap at $1.3 \pm 0.6\%$ strain (Supporting Information). PL intensity of bilayer A peak (unfilled circles) with no measurable change in intensity. Each color represents a distinct device. (b) GW_0 calculations of the fundamental band gaps of strained monolayer MoS_2, with an expected degeneracy at $\sim$5% strain. Optical band gap calculated by including the exciton binding energy yields a degeneracy at $\sim$0.1%.

To understand our experimental results, we compare them to the results of GW_0-BSE calculations; details are given in the Supporting Information. Crucially, these calculations capture the effect of strong electron−electron interactions in MoS_2 leading to the formation of excitons with binding energies significantly exceeding k_BT at room temperature.[28,29] This is important because PL spectroscopy probes the optical band gap: the difference between the fundamental (or transport) band gap and the exciton binding energy.

The observed redshift of the PL peaks is indicative of strain-induced reduction of band gaps in both monolayer and bilayer MoS_2. Indeed, our GW_0-BSE calculations for a monolayer

predict a reduction of the optical band gap at a rate of $\sim$59 meV/% strain (dashed line in Figure 3b), in close agreement with the measured PL peak shift. In bilayer devices, the calculated rates of reduction for the direct (67 meV/% strain) and indirect (94 meV/% strain) optical band gaps (dashed lines in Figure 3d) are also in close agreement with measured redshift rates for A and I peaks, 53 ± 10 and 129 ± 20 meV/% strain, respectively.

We interpret the rapid decrease in PL intensity of monolayer MoS_2 with strain as a signature of the anticipated strain-induced transformation of the *optical* band gap of this material from direct to indirect.[13,14,18,19] Indeed, at zero strain the energy difference between the minimum of the conduction band at the K point and the local maximum of the valence band at the Γ point (the indirect gap) is higher in energy than the direct gap at the K point (Figure 3a, inset, black curve). However, we calculate that the indirect gap reduces with strain faster than the direct gap (59 vs 94 meV/% strain). As a result, if we ignore the effect of excitons, at $\varepsilon \sim$5% the indirect gap overtakes the direct gap, and monolayer MoS_2 becomes an indirect-gap material. With excitonic effects included, our calculations indicate that the direct and indirect *optical* gaps (fundamental gaps minus binding energy of corresponding excitons) become degenerate at a much lower strain, 0.1% (Figure 4b). We, however, note that the accuracy of this value sensitively depends on the precise binding energy of the direct and indirect excitons that have not yet been measured experimentally.

As monolayer MoS_2 is strained and transitions from a direct to an indirect band gap material, we expect a marked decrease in the intensity of the A peak, as a majority of the excitons would not reside in this higher energy excitonic state, in good agreement with the decrease in intensity in Figure 4a. Quantitatively, a simple model describing direct and indirect excitons in monolayer MoS_2 as a two-level system yields an

acceptable fit to our experimental data (dashed curve in Figure 4a), with a direct-to-indirect band gap transition at $1.3 \pm 0.6\%$ strain (details in Supporting Information).

The observed PL spectra warrant two more comments. First, while for strains where the indirect band gap of monolayer MoS_2 is lower in energy than the direct band gap, we do not observe a peak corresponding to an indirect transition in its PL spectrum. This is likely due to the much smaller intensity of the indirect photoluminescence compared to the intensity of hot luminescence of the A peak. Second, in the range of strains from 1.3−5%, monolayer MoS_2 enters a curious regime where its fundamental band gap is direct, while the optical band gap is indirect.

In conclusion, we have observed strain-induced phonon softening, band gap modulation, and a transition from an optically direct to an optically indirect material in strained MoS_2 samples. These observations support a view of strain engineering as an enabling tool to both explore novel physics in MoS_2 (and other two-dimensional transition metal dichalcogenides such as $MoSe_2$, WS_2, and WSe_2) and to tune its optical and electronic properties. An interesting avenue of research would be to explore the regime of degenerate direct and indirect bands that play key roles in a plethora of spin-related properties of the MoS_2.[30,31] Among the potential applications of the strain-dependent photoluminescence of MoS_2 and its cousins are nanoscale stress sensors and tunable photonic devices: LEDs, photodetectors, and electro-optical modulators.

Note: While the manuscript was under review, two studies reporting modification of the band gap with strain became available.[32,33] The measured band gap shifts with strain are in general agreement with our results; however, because of the much lower range of strains employed in the devices of refs 32 and 33, they do not measure the Grüneisen parameter, probe the direct-to-indirect optical band gap transition, or observe contribution of excitonic effects.

■ ASSOCIATED CONTENT

Ⓢ Supporting Information

Bilayer Raman data, details of first-principles calculations, and a simple two-level model to calculate the intensity of strained MoS_2. This material is available free of charge via the Internet at http://pubs.acs.org.

■ AUTHOR INFORMATION

Corresponding Author
*(K.I.B.) E-mail: kirill.bolotin@vanderbilt.edu.

Notes
The authors declare no competing financial interest.

■ ACKNOWLEDGMENTS

■ REFERENCES

(1) Wang, Q. H.; Kalantar-Zadeh, K.; Kis, A.; Coleman, J. N.; Strano, M. S. Electronics and optoelectronics of two-dimensional transition metal dichalcogenides. *Nat. Nanotechnol.* **2012**, *7*, 699−712.

(2) Mak, K.; Lee, C.; Hone, J.; Shan, J.; Heinz, T. Atomically thin MoS_2: A new direct-gap semiconductor. *Phys. Rev. Lett.* **2010**, *105*, 2−5.

(3) Splendiani, A.; Sun, L.; Zhang, Y.; Li, T.; Kim, J.; Chim, C.-Y.; Galli, G.; Wang, F. Emerging photoluminescence in monolayer MoS_2. *Nano Lett.* **2010**, *10*, 1271−5.

(4) Radisavljevic, B.; Radenovic, A.; Brivio, J.; Giacometti, V.; Kis, A. Single-layer MoS_2 transistors. *Nat. Nanotechnol.* **2011**, *6*, 147−50.

(5) Lin, M.-W.; Liu, L.; Lan, Q.; Tan, X.; Dhindsa, K. S.; Zeng, P.; Naik, V. M.; Cheng, M. M.-C.; Zhou, Z. Mobility enhancement and highly efficient gating of monolayer MoS_2 transistors with polymer electrolyte. *J. Phys. D: Appl. Phys.* **2012**, *45*, 345102.

(6) Yin, Z.; Li, H.; Li, H.; Jiang, L.; Shi, Y.; Sun, Y.; Lu, G. Single-layer MoS_2 phototransistors. *ACS Nano* **2012**, *6*, 74−80.

(7) Sundaram, R. S.; Engel, M.; Lombardo, A.; Krupke, R.; Ferrari, A. C.; Avouris, P.; Steiner, M. Electroluminescence in single layer MoS_2. *Nano Lett.* **2013**, *13*, 1416−1421.

(8) Newaz, A. K. M.; Prasai, D.; Ziegler, J. I; Caudel, D.; Robinson, S.; Haglund, R. F., Jr.; Bolotin, K. I. Electrical control of optical properties of monolayer MoS_2. *Solid State Commun.* **2013**, *155*, 49−52.

(9) Ross, J. S.; Wu, S.; Yu, H.; Ghimire, N. J.; Jones, A. M.; Aivazian, G.; Yan, J.; Mandrus, D. G.; Xiao, D.; Yao, W.; Xu, X. Electrical control of neutral and charged excitons in a monolayer semiconductor. *Nat. Commun.* **2013**, *4*, 1474.

(10) Mak, K. F.; He, K.; Lee, C.; Lee, G. H.; Hone, J.; Heinz, T. F.; Shan, J. Tightly bound trions in monolayer MoS_2. *Nat. Mater.* **2013**, *12*, 207−11.

(11) Huang, M.; Yan, H.; Chen, C.; Song, D.; Heinz, T. F.; Hone, J. Phonon softening and crystallographic orientation of strained graphene studied by Raman spectroscopy. *Proc. Natl. Acad. Sci. U.S.A.* **2009**, *106*, 7304−8.

(12) Mohiuddin, T.; Lombardo, A.; Nair, R.; Bonetti, A.; Savini, G.; Jalil, R.; Bonini, N.; Basko, D.; Galiotis, C.; Marzari, N.; Novoselov, K.; Geim, A.; Ferrari, A. Uniaxial strain in graphene by Raman spectroscopy: G peak splitting, Grüneisen parameters, and sample orientation. *Phys. Rev. B* **2009**, *79*, 1−8.

(13) Lu, P.; Wu, X.; Guo, W.; Zeng, X. C. Strain-dependent electronic and magnetic properties of MoS_2 monolayer, bilayer, nanoribbons and nanotubes. *Phys. Chem. Chem. Phys.* **2012**, *14*, 13035−40.

(14) Pan, H.; Zhang, Y.-W. Tuning the electronic and magnetic properties of MoS_2 nanoribbons by strain engineering. *J. Phys. Chem. C* **2012**, *116*, 11752−11757.

(15) Yue, Q.; Kang, J.; Shao, Z.; Zhang, X.; Chang, S.; Wang, G.; Qin, S.; Li, J. Mechanical and electronic properties of monolayer MoS_2 under elastic strain. *Phys. Lett. A* **2012**, *376*, 1166−1170.

(16) Li, T. Ideal strength and phonon instability in single-layer MoS_2. *Phys. Rev. B* **2012**, *85*, 235407.

(17) Scalise, E.; Houssa, M.; Pourtois, G.; Afanas'ev, V.; Stesmans, A. Strain-induced semiconductor to metal transition in the two-dimensional honeycomb structure of MoS_2. *Nano Res.* **2012**, *5*, 43−48.

(18) Shi, H.; Pan, H.; Zhang, Y.-W.; Yakobson, B. I. Quasiparticle band structures and optical properties of strained monolayer MoS_2 and WS_2. *Phys. Rev. B* **2013**, *87*, 155304.

(19) Feng, J.; Qian, X.; Huang, C.; Li, J. Strain-engineered artificial atom as a broad-spectrum solar energy funnel. *Nat. Photonics* **2012**, *6*, 2−8.

(20) Bertolazzi, S.; Brivio, J.; Kis, A. Stretching and breaking of ultrathin MoS_2. *ACS Nano* **2011**, *5*, 9703−9.

(21) Novoselov, K. S.; Jiang, D.; Schedin, F.; Booth, T. J.; Khotkevich, V. V.; Morozov, S. V.; Geim, A. K. Two-dimensional atomic crystals. *Proc. Natl. Acad. Sci. U.S.A.* **2005**, *102*, 10451−10453.

(22) Li, H.; Zhang, Q.; Yap, C. C. R.; Tay, B. K.; Edwin, T. H. T.; Olivier, A.; Baillargeat, D. From bulk to monolayer MoS_2: evolution of raman scattering. *Adv. Funct. Mater.* **2012**, *22*, 1385−1390.

(23) Chen, C.; Rosenblatt, S.; Bolotin, K. I.; Kalb, W.; Kim, P.; Kymissis, I.; Stormer, H. L.; Heinz, T. F.; Hone, J. Performance of monolayer graphene nanomechanical resonators with electrical readout. *Nat. Nanotechnol.* **2009**, *4*, 861−7.

(24) Lee, C.; Yan, H.; Brus, L.; Heinz, T.; Hone, J.; Ryu, S. Anomalous lattice vibrations of single-and few-layer MoS_2. *ACS Nano* **2010**, *4*, 2695−2700.

(25) Rice, C.; Young, R. J.; Zan, R.; Bangert, U.; Wolverson, D.; Georgiou, T.; Jalil, R.; Novoselov, K. S. Raman-scattering measurements and first-principles calculations of strain-induced phonon shifts in monolayer MoS_2. *Phys. Rev. B* **2013**, *87*, 081307.

(26) Kern, G.; Kresse, G.; Hafner, J. Ab initio calculation of the lattice dynamics and phase diagram of boron nitride. *Phys. Rev. B* **1999**, *59*, 8551−8559.

(27) Sanjurjo, J. A.; López-Cruz, E.; Vogl, P.; Cardona, M. Dependence on volume of the phonon frequencies and the ir effective charges of several III-V semiconductors. *Phys. Rev. B* **1983**, *28*, 4579−4584.

(28) Cheiwchanchamnangij, T.; Lambrecht, W. R. Quasiparticle band structure calculation of monolayer, bilayer, and bulk MoS_2. *Phys. Rev. B* **2012**, *85*, 1−4.

(29) Ramasubramaniam, A. Large excitonic effects in monolayers of molybdenum and tungsten dichalcogenides. *Phys. Rev. B* **2012**, *86*, 115409.

(30) Mak, K. F.; He, K.; Shan, J.; Heinz, T. F. Control of valley polarization in monolayer MoS_2 by optical helicity. *Nat. Nanotechnol.* **2012**, *7*, 494−498.

(31) Zeng, H.; Dai, J.; Yao, W.; Xiao, D.; Cui, X. Valley polarization in MoS_2 monolayers by optical pumping. *Nat. Nanotechnol.* **2012**, *7*, 490−3.

(32) He, K.; Poole, C.; Mak, K. F.; Shan, J. Experimental demonstration of continuous electronic structure tuning via strain in atomically thin MoS_2. *Nano Lett.* **2013**, *13*, 2931−2936.

(33) Wang, G.; Zhu, C.; Liu, B.; Marie, X.; Feng, Q.; Wu, X.; Fan, H.; Tan, P.; Amand, T.; Urbaszek, B. Strain tuning of optical emission energy and polarization in monolayer and bilayer MoS_2. *arXiv:1306.3442* **2013**.